Stabilization of Absolute Instabilities in the Gyrotron Traveling Wave Amplifier

K. R. Chu,[1] L. R. Barnett,[1] H. Y. Chen,[1] S. H. Chen,[2] Ch. Wang,[3] Y. S. Yeh,[1] Y. C. Tsai,[1] T. T. Yang,[3] and T. Y. Dawn[2]

[1]*Department of Physics, National Tsing Hua University, Hsinchu, Taiwan*

[2]*Department of Nuclear Engineering, National Tsing Hua University, Hsinchu, Taiwan*

[3]*RF Group, Synchrotron Radiation Research Center, Hsinchu, Taiwan*

(Received 17 June 1994)

Absolute instabilities in the gyrotron traveling wave amplifier are investigated with a simulation approach which models electron and wave dynamics in the sever and distributed-loss section. Distributed wall losses are shown to be far more effective than the sever in stabilizing these instabilities. Physical interpretations are given and theoretical predictions are verified by a K_a-band experiment which achieved 62 kW peak power with 12% bandwidth, 21% efficiency, and 33 dB saturated gain through the use of a mechanically adjustable magnetron injection gun.

PACS numbers: 42.52.+x, 85.10.Jz

The gyrotron traveling wave tube amplifier (gyro-TWT) promises a new generation of high power, broadband, millimeter-wave amplifiers. The Naval Research Laboratory [1–3] reported a 35 GHz, TE_{01} mode gyro-TWT with 16.6 kW output power, 20 dB gain, 7.8% efficiently, and 1.5% FWHM bandwidth. In the C band, 120 kW with 18 dB gain, 26% efficiency, and 6% bandwidth was achieved by Varian Associates [4]. Oscillations due to absolute instabilities (those occurring in the backward wave branches or near the cutoff points) in the gyro-TWT have been a major physics limitation [1–10] in the realization of its ultimate capability. Additional limiting factors include the demand of a high quality electron beam and wide band couplers with low reflections. Research in recent years has yielded much insight into the physical mechanisms of absolute instability competition/suppression [8–10] and reflection-induced oscillations [11,12], which led to the suggestion of a two-stage interaction structure as a possible remedy [9,12–16]. In the K_a band, the National Tsing Hua University obtained 27 kW power with 35 dB gain, 16% efficiency, and 7% bandwidth in a severed circuit [9], while the Naval Research Laboratory achieved 8 kW with 25 dB gain, 16% efficiency, and an impressive 20% bandwidth by combining a sever with tapered waveguides [13]. Interestingly, harmonic gyro-TWT's have been shown to be more stable against absolute instabilities [14–16]. A second harmonic K_u-band gryro-TWT experiment has recently demonstrated 207 kW power with 16 dB gain, 13% efficiency, and 2.1% bandwidth [17]. In this Letter, we present theoretical and experimental investigations on the physical mechanisms involved in the stabilization of absolute instabilities by the sever [9,12–16] and distributed wall losses [3,4]. In the experiment, the electron beam quality was controlled through the use of a mechanically adjustable magnetron injection gun (MIG).

We first describe an innovative version of the MIG (Fig. 1) which features mechanical adjustability of its focusing electric field. Because of its proximity to the electron emitter and its location in the high electric field region, the cathode nose mounted on the tip of a sliding rod (Fig. 1) provides an effective means for local field adjustment. Trajectory simulations for the MIG configuration of Fig. 1 indicate a strong sensitivity of the beam quality (characterized by the axial velocity spread $\Delta\nu_z/\nu_z$) with respect to the axial position of the cathode nose relative to the rest of the cathode [Fig. 2(a)]. A slight shift of the nose position may result in a large variation in the α value and beam quality, while the nose position for the best beam quality changes with the beam current I_b. The α value ($= \nu_\perp/\nu_z$) can also be adjusted within a modest range [Fig. 2(b)]. Thus the adjustability of the nose position provides an extra, and often critical, degree of freedom for the optimization of the beam quality as well as compensation for machining errors and thermal deformations, providing the versatility of operation in a much greater parameter space.

A two-stage interaction structure separated by a sever has been analyzed [12–16] and implemented [9,13] at low beam currents ($I_b < 1.8$ A) for stable operation of gyro-TWT's. However, at higher beam currents ($I_b > 2$ A), absolute instabilities, multiple reflections, and coupling between the two stages were often the causes for the experimentally observed oscillations, interference ripples, and poor efficiency. To remedy these problems, there is clearly a need for improved modeling which accounts for details of the wave behavior and electron dynamics inside the sever.

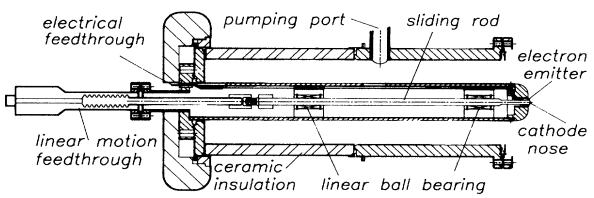

FIG. 1. Cathode assembly of a mechanically adjustable magnetron injection gun.

0031-9007/95/74(7)/1103(4)$06.00

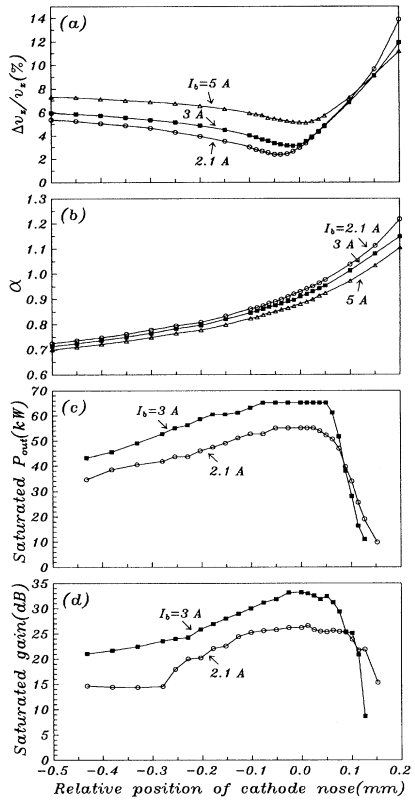

FIG. 2. Simulated beam velocity spread (a) and α value (b) as functions of the axial position of the cathode nose relative to the rest of the cathode. (c) and (d) display the measured gyro-TWT output power and gain as functions of the cathode nose position. For f = 34.3 GHz, V_b = 99.45 kV, and B_0/B_g = 0.99.

We have developed a single-mode code to investigate sever effects as well as alternative methods for achieving a stable tube. The code is based on the commonly used technique of steady-state particle tracing in a weakly nonuniform interaction structure. The transverse mode profile is approximated by that of a uniform guide, while the axial mode profile is self-consistently calculated. A new element of the formalism is the incorporation of a loss factor [18] valid for all frequencies (including the cutoff) to model wall losses. Wave behavior can then be followed throughout the sever instead of being artificially set to zero in the sever as in earlier models [12–16]. This improvement makes it possible to treat two important physical effects (examples shown later): (1) wave reflection off and transmission through the sever, which provide the feedback and coupling mechanisms to cause interference ripples at low beam currents and self-oscillations at high beam currents; and (2) beam-wave interaction inside the sever, which provides the self-consistent connection between the dynamics in the two stages. Another new capability of the code is that, through proper setting of boundary conditions, it works in either the amplification or self-oscillation mode.

With the help of the code, behavior of absolute instabilities in the severed gyro-TWT [Fig. 3(a)] has been better understood. The two stages, though separated by the sever, are coupled by the beam. Thus, for the absolute instabilities for which the beam provides an internal feedback path, the sever does not really quite cut the interaction waveguide into two independent sections to produce a substantial stabilizing effect. This has motivated us to turn to the interaction structure shown in Fig. 3(b) where the wall losses are distributed over approximately the first half of the waveguide, producing a total circuit loss of ~20 dB at the band center. With such a structure, the interaction length is truly shortened by the length of the lossy section. Amplification of the TE_{11} mode in the structure of Fig. 4(a) and 4(b) at a frequency (34.2 GHz) near the band center has been studied with the new code for the following parameters: V_b = 99.5 kV, I_b = 3 A, α = 0.85, $\Delta v_z/v_z$ = 5%, electron guiding center r_c at 0.09 cm, and a uniform magnetic field B_0 at 0.99 of the grazing value B_g. The forward power (P_{fwd}) and the corresponding gain [$= 10\log_{10}(P_{\mathrm{fwd}}/P_{\mathrm{in}})$] are plotted as a function of the axial position in Fig. 4(c). The wave grows in the lossy section by ~13 dB as it emerges into the copper section. The forward power at the output end (P_{out} ~ 60 kW) corresponds to a saturated gain of ~33 dB and an efficiency ($\eta = P_{\mathrm{out}}/I_b V_b$) of ~20%.

The behavior of the reflected wave (P_{rf1}) is diagnosed in Fig. 4(d). The reflected wave is seen to originate from the output taper. As it propagates backward, it beats with the forward wave. Upon entering the lossy section, it starts to attenuate and eventually ~99% of the power dissipates into the wall. Ohmic loss along the tube is diagnosed in Fig. 4(e). The total dissipated power is 1.1% of the beam power, and it is about evenly divided between the lossy and copper sections, which optimizes the tube's power-handling capability. Like the sever, the lossy section cuts off the path of the reflected wave. However, in contrast to the sever, the lossy section has a much lower wall

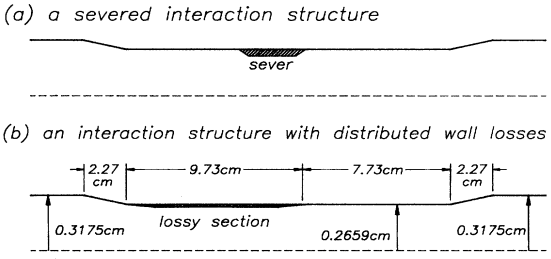

FIG. 3. (a) Schematic of a severed interaction structure and (b) a TE_{11} mode interaction structure with distributed wall losses (used in subsequent experiment). Tapers at the ends are to broaden the coupler bandwidth.

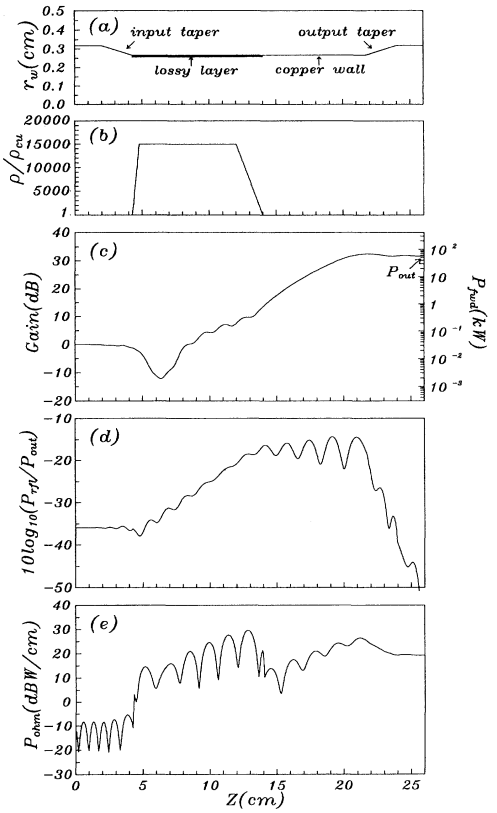

FIG. 4. Model and theoretical analysis (at $f = 34.2$ GHz) of a TE_{11} mode, fundamental harmonic gyro-TWT with distributed wall losses. (a) Wall profile. (b) Normalized wall resistivity versus the axial position z, $\rho_{Cu} = 1.72 \times 10^{-8}\ \Omega$ m. (c) Forward wave power (P_{fwd}) and gain versus z. (d) Reflected wave power (P_{rfl}, normalized to P_{out}) versus z. (e) Ohmic loss versus z. $V_b = 99.5$ kV, $I_b = 3$ A, $\alpha = 0.85$, $\Delta\nu_z/\nu_z = 5\%$, $r_c = 0.09$ cm, and $B_0/B_g = 0.99$.

resistivity such that the drive wave can still be amplified in it [Fig. 4(c)].

Figure 5 compares the calculated self-oscillation thresholds of the most likely absolute instability (TE_{21} oscillation at the second cyclotron harmonic) for the unsevered, severed, and distributed-loss interaction circuits of identical total length and operating parameters (as in Fig. 4). The start oscillation currents for the three cases are, respectively, 0.1, 0.9, and 26 A. The first two cases are in good agreement with the experiments in Refs. [8] and [9], respectively. The last case represents complete stabilization of the most likely absolute instability, as will be corroborated by the experiment described below. The far stronger stabilizing effect of distributed losses can be attributed to the predominantly *backward* power flow of absolute instabilities. Hence, a lossy section located upstream serves as an effective damper to oscillations caused by absolute instabilities.

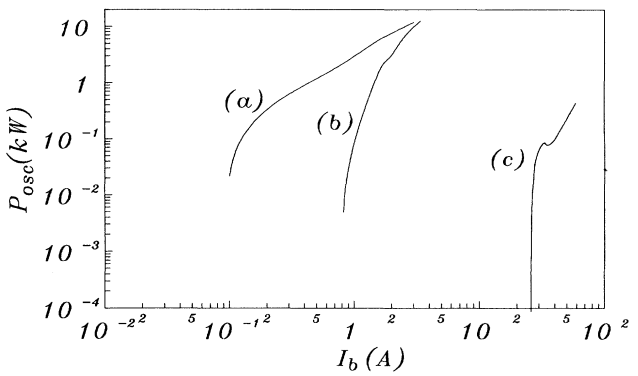

FIG. 5. Calculated self-oscillation power of the TE_{21} mode at the second cyclotron harmonic ($f \sim 56$ GHz) versus the beam current for (a) an unsevered tube [Fig. 3(a) without the sever], (b) a severed tube [Fig. 3(a)], and (c) a tube with distributed losses [Fig. 3(b)], all of the same total length and operating parameters as Fig. 4.

In the gyro-TWT experimental setup, the MIG of Fig. 1 was incorporated with the interaction circuit of Fig. 3(b). Input/output waves were coupled through the side walls [8]. The magnetic field was provided by a superconducting magnet system. The lossy section was coated with graphite material. Output power was measured with a calibrated crystal detector (with estimated accuracy of $\sim \pm 5\%$) and verified with a calorimeter (agreement was within $\sim 5\%$). The gyro-TWT was found to be (zero drive) stable from all absolute instabilities up to a (maximum possible) tested beam current of 6 A, which is still well under the predicted TE_{21} oscillation threshold (Fig. 5). Reflection-induced oscillation (at ~ 37 GHz) also had a much higher threshold than in previous cases and could be tuned away up to a beam current of ~ 3 A by adjustment of the cathode nose position. The desirability for the mechanical adjustability is seen in Figs. 2(c) and 2(d). For positions of the cathode nose marked by negative values, the α value increases and beam quality improves with a nose position increment, resulting in an increase in the measured power and gain [Figs. 2(c) and 2(d)]. As the nose was moved outward into positively marked positions, the beam quality started to deteriorate and the output power decreased. With the nose moved out further, the α value exceeded the threshold of reflection-induced oscillation and both power and gain dropped sharply [Figs. 2(c) and 2(d)].

Figure 6 displays the measured and calculated output power spectrum at saturation drive powers for the parameters of Fig. 4. The measured data show an instantaneous 3 dB bandwidth of $\sim 12\%$ with a peak power of ~ 62 kW at $\sim 21\%$ efficiency, giving a power-bandwidth product 2.5 times greater than that of the state-of-the-art K_a-band TWT's. The calculated power was in good agreement with the experiment except at the left band edge.

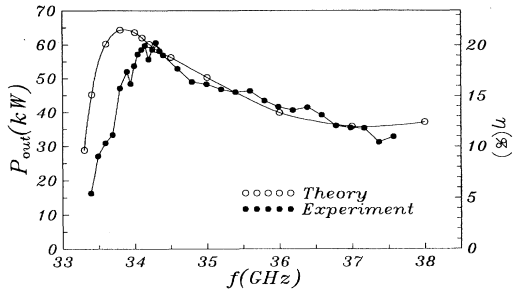

FIG. 6. Calculated and measured output power spectrum showing the instantaneous saturated bandwidth. Parameters are given in Fig. 4.

However, the comparison must be viewed in the context that the beam velocity spread and α value used in the calculation were based on MIG simulations rather than actual measurements.

In summary, a self-consistent treatment of the beam/wave dynamics in the sever and distributed-loss section has led to theoretical understanding and consequent experimental suppression of the absolute instabilities. Because of its internal origin, the absolute instability has been an intrinsic physics issue of the gyro-TWT. Removal of this limitation has opened the possibility for a new source with unprecedented capability. Oscillation due to the forwardly convective TE_{11} instability, on the other hand, has an *external* origin. It results from reflections occurring at the mismatched input/output couplers [Fig. 4(d)]. The distributed loss was also effective in suppressing reflection-induced TE_{11} oscillations, but only up to a beam current of ~3 A in the present experiment. This was the primary reason for the upper bound in the power achieved. Judging from the origin of the reflected wave, the next required step appears to be an innovation in the input/output couplers to minimize reflections.

This work was sponsored by the National Science Council under Contract No. NSC83-0208-M-007-036. The authors are grateful for helpful discussions with Dr. H. Guo.

[1] J.L. Seftor, V.L. Granatstein, K.R. Chu, P. Sprangle, and M.E. Read, IEEE J. Qantum Electron. **15**, 848 (1979).

[2] L.R. Barnett, K.R. Chu, J.M. Baird, V.L. Granatstein, and A.T. Drobot, in *Technical Digest of the International Electron Devices Meeting* (IEEE, New York, 1979), pp. 164–167.

[3] L.R. Barnett, J.M. Baird, Y.Y. Lau, K.R. Chu, and V.L. Granatstein, in *Technical Digest of the International Electron Devices Meeting* (IEEE, New York, 1980), pp. 314–317.

[4] R.S. Symons, H.R. Jory, S.J. Hegji, and P.E. Ferguson, IEEE Trans. Microwave Theory Tech. **29**, 181 (1981).

[5] Y.Y. Lau, K.R. Chu, L.R. Barnett, and V.L. Granatstein, Int. J. Infrared Millimeter Waves **2**, 373 (1981).

[6] K.R. Chu and A.T. Lin, IEEE Trans. Plasma Science **16**, 90 (1988).

[7] A.T. Lin and P.K. Kaw, Int. J. Electron. **72**, 884 (1992).

[8] L.R. Barnett, L.H. Chang, H.Y. Chen, K.R. Chu, Y.K. Lau, and C.C. Tu, Phys. Rev. Lett. **63**, 1062 (1989).

[9] K.R. Chu, L.R. Barnett, W.K. Lau, L.H. Chang, and C.S. Kou, in *Technical Digest of International Electron Devices Meeting* (IEEE, New York, 1990), pp. 699–702.

[10] K.R. Chu, L.R. Barnett, W.K. Lau, L.H. Chang, A.T. Lin, and C.C. Lin, Phys. Fluids B **3**, 2403 (1991).

[11] G.S. Park, S.Y. Park, R.H. Kyser, A.K. Ganguly, and C.M. Armstrong, in *Technical Digest of International Electron Drive Meeting* (IEEE, New York, 1990), pp. 703–705; in *Technical Digest of International Electron Device Meeting* (IEEE, New York, 1991), pp. 779–781.

[12] A.K. Ganguly and S. Ahn, Int. J. Electronics **53**, 641 (1982); IEEE Trans. Electron Devices **31**, 474 (1984).

[13] G.S. Park, J.J. Choi, S.Y. Park, C.M. Armstrong, A.K. Ganguly, and R.H. Kyser, in *Technical Digest of International Electron Device Meeting* (IEEE, New York, 1993), pp. 351–353.

[14] A.T. Lin, K.R. Chu, C.C. Lin, C.S. Kou, D.B. McDermott, and N.C. Luhmann, Jr., Int. J. Electron. **72**, 873 (1992).

[15] C.S. Kou, Q.S. Wang, D.B. McDermott, A.T. Lin, K.R. Chu, and N.C. Luhmann, Jr., IEEE Trans. Plasma Science **20**, 155 (1992).

[16] Q.S. Wang, C.S. Kou, D.B. McDermott, A.T. Lin, K.R. Chu, and N.C. Luhmann, Jr., IEEE Trans. Plasma Science **20**, 163 (1992).

[17] Q.S. Wang, K.C. Leou, C.K. Chong, A.J. Balkcum, D.B. McDermott, and N.C. Luhmann, Jr., in Digest of the 19th International Conference on Infrared and Millimeter Waves, Sendai, Japan, 1994, edited by K. Sakai and T. Yoneyama (unpublished), pp. 415–6.

[18] K.R. Chu, C.S. Kou, J.M. Chen, Y.C. Tsai, C. Cheng, S.S. Bor, and L.H. Chang, Int. J. Infrared Millimeter Waves **13**, 1571 (1992).